Stress evaluation of crystalline polymers using X-ray diffractometry

Akimitsu Nezu* and Takuya Kikuchi**

Abstract

As the demand for environmental sustainability and energy conservation continues to grow, lightweight structural design has become increasingly important in transportation systems such as automobiles. Engineering plastics are being adopted as alternatives to steel because of their advantageous mechanical properties. However, residual stress introduced during molding can adversely affect structural stability, making quantitative evaluation essential. This study investigates the applicability of X-ray diffraction for evaluating residual stresses in polyacetal.

1. Introduction

Global environmental concerns and energy efficiency demands are driving efforts to reduce structural component weight in transportation systems and electronic devices. This is particularly evident in the automotive industry, where the number of vehicles in use worldwide is expected to continue rising. Accordingly, lightweight structural design is essential for improving fuel efficiency and reducing CO_2 emissions, thereby minimizing environmental impact.

A significant trend to address this challenge is the replacement of certain components traditionally made from steel with lightweight metals or high-strength polymer materials. Among these, engineering plastics have attracted considerable attention as materials that combine high specific strength, heat resistance, chemical resistance, and moldability, and they have already been applied to structural components in practice.

However, residual stress generated during the molding of polymer materials can lead to reduced fatigue strength and dimensional changes. Although knowledge and data remain insufficient, industrial applications have already begun, creating a strong need for the quantitative evaluation of residual stress from the perspective of structural stability and safety. However, the evaluation of residual stress in polymer materials faces challenges arising from material properties and measurement principles, and methods for addressing these challenges are not yet well established.

Although the ultimate goal is to evaluate residual stress in actual products, this study first examines the feasibility and accuracy of X-ray stress measurement for polymer materials through tensile stress measurements on test specimens, focusing on polyacetal (POM), one of the representative engineering plastics.

*Application Laboratories, Rigaku Corporation.
**XRD Product Division, Rigaku Corporation.

2. Engineering Plastics

2.1. Properties of Polyacetal (POM)

Polymers, including synthetic resins and plastics, are broadly classified into two categories: thermoplastics and thermosets. Thermoplastic resins melt at elevated temperatures and solidify upon cooling. Even after solidification, they can be remelted by reheating, which demonstrates reversible thermal behavior and allows repeated processing. In contrast, thermosetting resins solidify upon heating and, once set, retain their form regardless of subsequent heating or cooling.

Here, we focus on engineering plastics within the thermoplastic category, particularly polyacetal, which is a crystalline resin with a periodic molecular arrangement[(1)–(3)].

Polyacetal is widely used as a metal substitute because of its high mechanical strength and dimensional stability compared to other engineering plastics. In terms of mechanical properties, it exhibits high tensile strength (60–70 MPa) and tensile modulus (2.5–3.0 GPa), while its specific gravity is about 1.41, making it relatively lightweight. As a result, it demonstrates performance comparable to that of metallic materials in terms of specific strength and specific rigidity. Furthermore, its low coefficient of friction (0.2–0.3) and high wear resistance make it highly suitable for sliding components. It also has excellent impact resistance and high durability against repeated loads, which is why it is used in parts such as gears and bearings. Another notable feature is its high dimensional stability; due to its low water absorption, dimensional changes caused by humidity or temperature fluctuations are minimal, enabling its use in precision components. In addition, it offers excellent chemical and oil resistance, remaining stable against many organic solvents and oils. However, it is susceptible to strong acids and bases, so care must be taken regarding the operating environment. To further promote its practical application as a metal substitute, improvements in heat resistance, weatherability, and recyclability are essential. In recent years, advances have been made in composite technologies such as

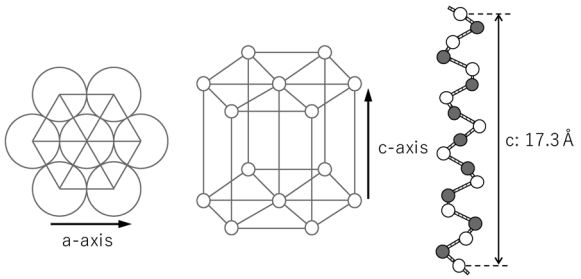

Fig. 1. Crystal structure of POM.

the addition of fibers or nanofillers and the creation of polymer alloys with different resin types, leading to further enhancements in mechanical properties and functionality.

Polyacetal is a crystalline polymer, and its molecular chains are regularly and densely packed, resulting in a high degree of crystallinity and, consequently, high rigidity and dimensional stability. As shown in Fig. 1, its crystal structure consists of molecular chains, each comprising nine [–CH_2O–] units forming five helical turns aligned along the c-axis. It belongs to the hexagonal crystal system (space group $P3_1$, No. 144). There are mainly two types: homopolymer (POM-H) and copolymer (POM-C). POM-H has a higher degree of crystallinity and mechanical strength, while POM-C offers superior heat resistance and hydrolysis resistance.

During injection molding, the molten resin rapidly fills the mold and cools quickly. In this process, the molecular chains are primarily oriented along the flow direction (MD direction), and crystallization progresses. Rapid cooling in the surface layer of the molded product leads to strong molecular orientation, whereas slower cooling in the core results in more random orientation. This layered (skin-core) structure significantly affects the mechanical properties and dimensional stability of the molded product. The degree of molecular orientation varies depending on molding conditions such as injection speed, mold temperature, resin temperature, and holding time. Higher injection speeds or lower mold temperatures result in stronger orientation, improving rigidity and wear resistance but reducing impact strength and dimensional stability. Conversely, molding conditions that produce less orientation tend to yield more uniform properties throughout the molded product. Controlling molecular orientation in this way is important for maximizing the functionality of polymer materials. In recent years, advances in molding simulation technology and orientation analysis using X-ray diffraction or polarized light microscopy have enabled more precise design of molded products.

2.2. Test Specimens

The test specimens were made from polyacetal (model M90-44) manufactured by Polyplastics Co., Ltd., and were prepared as dog-bone-shaped tensile specimens with a gauge length of l_1=24 mm, a width of b_1=3.5 mm, and a thickness of t=2 mm, as shown

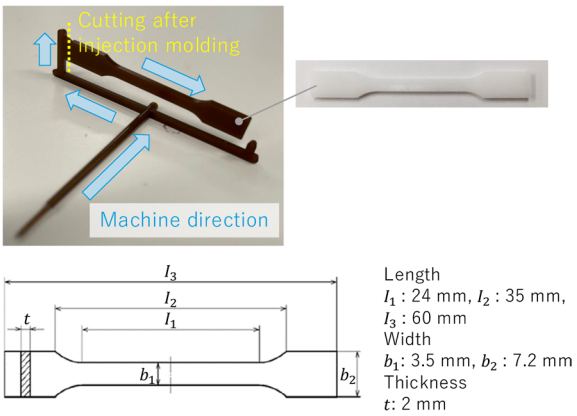

Fig. 2. Tensile test specimen of POM.

Table 1. Mechanical properties of POM (M90-44).

Density	Tensile strength	Tensile modulus	Flexural modulus
1.41 g/cm^3	62 MPa	2700 MPa	2500 MPa

Table 2. Thermal properties of POM (M90-44).

Coefficient of linear thermal expansion (23–55°C, MD)	Glass transition temperature
12×10^{-5}/°C	Around −50°C

in Fig. 2. These specimens were produced by injection molding, with the MD direction aligned with the specimen's longitudinal axis. The injection molding conditions were as follows: mold temperature of 80°C, cylinder temperature of 200°C, injection speed of 10 mm/s, and holding pressure of 60 MPa. One of the two specimens was annealed at 100°C for 3 hours under vacuum. To facilitate the evaluation of stress in crystalline polymers, and to aid in the interpretation of measurement results, filler-free material was used for the test specimens. Table 1 summarizes the mechanical properties of polyacetal (M90-44), and Table 2 shows its thermal properties[18].

3. Stress Measurement in Polymer Materials

3.1. Various Stress Measurement Techniques

In metallic and ceramic materials, atomic order and periodicity at the sub-nanometer scale extend to the bulk level, creating a strong correlation between microscopic and macroscopic properties. In contrast, crystalline polymers exhibit hierarchical structures ranging from atomic-scale arrangements to nanometer- and micrometer-scale features such as lamellar crystals and spherulites, and further to macroscopic forms like fibers, films, or bulk materials. Structural variation at each level requires different property evaluations and analytical techniques[4, 5]. Here, we review stress measurement techniques applicable to polymer materials, which are increasingly employed as structural components[6].

The strain gauge method (SG), commonly used

for metals, is a mechanical technique that measures strain released when a specimen is cut or drilled. It can detect minute strains of several microstrains ($\mu\varepsilon$) on the attached surface, enabling highly accurate stress measurement. However, SG is classified as a destructive method, and accurate results depend on operator skill, including proper surface preparation and uniform gauge adhesion.

Raman spectroscopy (RS), like X-ray diffraction, is a non-destructive, non-contact technique effective for evaluating residual stress and molecular orientation in polymers. When strain is applied, molecular vibrational states change; when irradiated with a monochromatic laser, these changes appear as peak shifts in the Raman scattering spectrum. RS is particularly sensitive to carbon–carbon bond vibrations and offers high spatial resolution, enabling local analysis within micrometer-scale regions. However, Raman scattering is weak and highly susceptible to external noise, and materials with low Raman activity exhibit only minor peak shifts.

Other techniques include the bimetal method, which measures warpage of adherends bonded with resin adhesives, and the photoelastic method, which observes refractive index changes accompanying deformation of molded products. These techniques are selected based on specimen type, application, and field requirements.

3.2. X-ray Diffraction Method

The X-ray diffraction method (XRD) is a non-destructive, non-contact technique for analyzing crystalline structures, based on Bragg's diffraction condition ($2d\sin\theta = n\lambda$), where d is the lattice spacing, θ is the Bragg angle (half of the diffraction angle 2θ), and λ is the wavelength of the characteristic X-rays. XRD can be readily applied to a wide range of sample forms—including powders, bulk materials, films, fibers, liquids, and gels—without extensive sample preparation, making it widely used in both academic research and industrial applications.

This study focuses on changes in lattice spacing on the order of several angstroms that occur when strain is applied to polymers[7, 8]. X-ray diffraction measures the size and shape of crystal lattices; in other words, it can directly detect strains corresponding to lattice dimension changes of several angstroms. Therefore, the quantitative accuracy of stress and strain measurements by XRD is considered higher than that of other methods. However, due to its principle, the technique is fundamentally limited to crystalline materials. The analysis depth depends on factors such as the wavelength of the characteristic X-rays, the material's X-ray absorption coefficient, and the incident angle. In metals and ceramics, the analysis depth typically ranges from several micrometers to approximately 10 μm, while in polymers it extends from several tens to several hundreds of micrometers. Because the measurement provides an average of the crystalline state within this depth, a state of stress is assumed to be uniform throughout the X-ray penetration depth for analysis.

3.3. X-ray Stress Measurement Method ($\sin^2\psi$ Method)

First, we consider lattice strain. Unlike macroscopic strain, which can be determined from dimensional changes when a cylindrical rod is subjected to uniaxial tension, our focus here is on microscopic lattice strain that cannot be directly observed. Let d_0 denote the interplanar spacing in the strain-free state and d the interplanar spacing in the strained state; the lattice strain is then expressed as shown in Eq. (1). In other words, the ratio of the change in interplanar spacing to the strain-free value is defined as the lattice strain ε.

$$\varepsilon = \frac{d - d_0}{d_0} \tag{1}$$

The fundamental concept of X-ray stress measurement is to calculate the stress σ_{kl} using Hooke's law ($\varepsilon_{ij} = S_{ijkl}\sigma_{kl}$), based on the strain ε_{ij} measured by X-ray diffraction. The subscripts i, j, k, l indicate that stress and strain are second-order tensors, while the elastic constants are fourth-order tensors.

In this study, the widely used $\sin^2\psi$ method (the sin-squared-psi method) for X-ray stress measurement in polycrystalline materials was employed. Here, the angle ψ is defined as the angle between the specimen surface normal and the normal to the selected lattice plane. In the $\sin^2\psi$ method, a specific lattice plane (hkl) is selected, and the ψ angle is sequentially tilted in multiple orientations within the same plane to observe changes in the interplanar spacing d as a function of ψ. For example, when compressive residual stress is present, d decreases as ψ increases, causing the diffraction peak to shift to higher 2θ values according to Bragg's law. A plot of 2θ versus $\sin^2\psi$ (the 2θ–$\sin^2\psi$ diagram) is analyzed by linear regression, and the stress σ is obtained by multiplying the slope M of the regression line by the material-specific X-ray stress constant K. The fundamental equation of the $\sin^2\psi$ method is given in Eq. (2), where E is Young's modulus, ν is Poisson's ratio, and θ_0 is the Bragg angle in the strain-free state. The value of $2\theta_0$ is often referenced from the literature or powder diffraction databases.

$$\sigma = -\frac{E}{2(1+\nu)} \cdot \cot\theta_0 \cdot \frac{\pi}{180} \cdot \frac{\Delta(2\theta)}{\Delta(\sin^2\psi)}$$
$$\sigma = K \cdot \frac{\Delta(2\theta)}{\Delta(\sin^2\psi)} \tag{2}$$

The $\sin^2\psi$ method offers two main advantages. First, even if the value of d_0 is not precisely known, its error has little effect on the calculated stress, since the method uses the change in interplanar spacing with respect to ψ rather than the absolute value of strain. Second, the method measures the stress component σ_x in the direction of tilt. Therefore, it is important to appropriately select the specimen orientation and the tilting method (parallel-tilt or side-tilt), considering the direction of the external (principal) stress acting on the

specimen and the specimen geometry.

3.4. Challenges in X-ray Stress Measurement for Polymers

Here, we discuss the challenges associated with applying the $\sin^2\psi$ X-ray stress measurement method to polymer materials. To date, the $\sin^2\psi$ method has been most widely applied to metallic materials. One reason for this is that, in metals, diffraction peaks used for stress measurement can be observed at high angles ($2\theta > 100°$), which enables high strain sensitivity and precise measurement of peak shifts.

In contrast, crystalline polymers possess long-period structures and significant molecular fluctuations within the crystalline regions, which results in attenuation of diffraction intensity at high 2θ angles. As a result, sharp and intense diffraction peaks are typically observed only at low angles ($2\theta \approx 20$–$30°$). When comparing strain sensitivity at high and low 2θ angles, the difference is significant. Strain sensitivity can be expressed as shown in Eq. (3), where ε is the crystal strain, $\Delta\theta$ which is half the peak shift $\Delta 2\theta$, and θ_0 is the Bragg angle in the strain-free state. For example, if a peak shift of $\Delta 2\theta_1 = 1°$ occurs at $2\theta_1 = 156°$, and the same strain is measured at $2\theta_2 = 20°$, the corresponding peak shift is only $\Delta 2\theta_2 = 0.037°$, resulting in a strain sensitivity that is approximately 27 times greater at high angles than at low angles. Thus, a key challenge in polymer materials is that measurements must be performed under conditions of low strain sensitivity.

$$\varepsilon = -\Delta\theta \cdot \cot\theta_0 \tag{3}$$

Additionally, polymers are viscoelastic materials, and the elastic region showing linearity in the stress–strain curve is narrower and less distinct than in metals. As a result, the elastic strain to be measured by X-ray stress measurement is extremely small, which presents another challenge.

Furthermore, polymers have a lower absorption coefficient for X-rays compared to metals, resulting in greater X-ray penetration depth. Consequently, X-rays diffracted from both the surface and the interior of the specimen are detected together, potentially introducing angular errors in the diffraction peaks. For polyacetal, the X-ray penetration depth for Cu Kα radiation is estimated to be about 90 μm for the (100) reflection ($2\theta = 22.87°$) and about 135 μm for the (105) reflection ($2\theta = 34.53°$). These values are calculated under the condition $\mu t = 1$ in Lambert–Beer's law, assuming reflection geometry at $\psi = 0°$, where μ is the linear absorption coefficient and t is the X-ray penetration depth ($t = \tau$).

In summary, X-ray stress measurement in polymers requires the detection of extremely small peak shifts under conditions of low strain sensitivity. Therefore, to address these challenges, X-ray diffractometers must be equipped with: (1) highly parallel incident X-rays to eliminate angular errors, (2) a measurement optical system with high 2θ angular resolution capable of detecting minute peak shifts, and (3) a high-precision goniometer with a side-inclination axis for tilting ψ angles at low 2θ diffraction peaks.

In this study, we used the SmartLab X-ray diffractometer (Rigaku, Japan), which can be configured with various measurement optics as a multipurpose instrument and is equipped with a horizontal sample goniometer. Figure 3 shows the measurement optical system for the parallel beam (PB) method using SmartLab. (1) The X-ray source is a Cu-sealed ceramic tube (Long Fine Focus, 2.2 kW) with a line focus orientation. (2) The CBO (Cross Beam Optics) unit, equipped with a Si/W multilayer mirror, forms a parallel beam by reflection from a parabolic mirror. (3) A 0.5 mm slit for micro-area measurement and a ϕ0.8 mm short collimator are used. (4) A tensile testing machine is used for tensile stress measurements; details are described in Section 4.2.1. (5) The PSA (Parallel Slit Analyzer), consisting of thin metal plates aligned in the 2θ direction, allows only highly parallel diffracted X-rays to pass, eliminating divergent components; here, a PSA with an aperture angle of 0.5° was used. (6) The HyPix-3000 pixel array semiconductor detector, which can be switched between 0D/1D/2D modes, is employed. (7) A χ (chi) cradle is used for stress measurement using the side-inclination method.

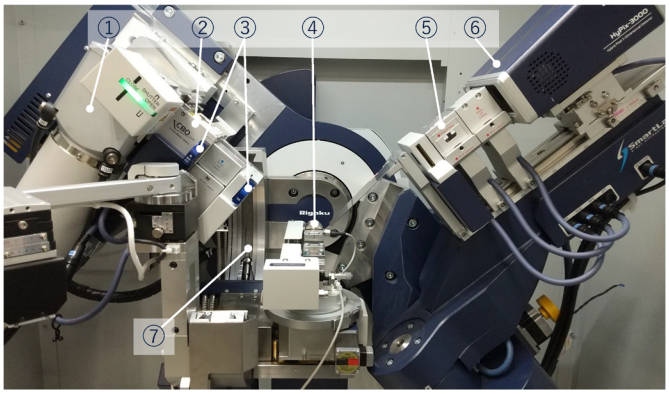

(a)Actual goniometer used for the PB optical system.

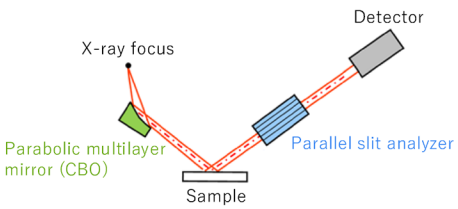

(b)Schematic of the PB optical system.

Fig. 3. Measurement optical system for the PB method using SmartLab.

4. Results and Discussion

4.1. X-ray Diffraction Measurements

4.1.1. X-ray Diffraction Pattern Measurement (0D)

Figure 4 shows the X-ray diffraction patterns of the untreated and annealed polyacetal specimens measured using the parallel beam method. The scan conditions for the $\theta/2\theta$ scan are summarized in Table 3. By comparing the full width at half maximum (FWHM) of the (100) diffraction peak in Fig. 4, it is observed that the untreated specimen shows a FWHM of 0.495°, while the annealed specimen shows a reduced FWHM of 0.482°, indicating a decrease in peak width after annealing. This suggests that crystallization was slightly promoted by the annealing treatment.

Focusing on the five sharp crystalline peaks and one broad amorphous peak (halo) observed in Fig. 4, the degree of crystallinity was analyzed using the peak fitting method, and the results showed a crystallinity of 77.1 vol% for the untreated specimen and 77.4 vol% for the annealed specimen. Here, the degree of crystallinity V_c is defined as shown in Eq. (4). Additionally, Fig. 5 shows the result of peak separation for the annealed specimen using the whole powder pattern fitting (WPPF) method (R_{wp}=4.37%, S=1.01) as supplementary information. These results indicate that polyacetal is a resin capable of achieving relatively high crystallinity compared to other resins.

$$V_c = \frac{\sum(\text{Scattering intensity of crystalline phase})}{\sum(\text{Scattering intensity of crystalline phase}) + \sum(\text{Scattering intensity of amorphous})} \quad (4)$$

Furthermore, by comparing the relative integrated intensities of the observed crystalline peaks with those listed in the powder diffraction database (ICDD2025, PDF-2), the orientation state was qualitatively estimated. The orientation degree was found to be 27.6 vol% for the untreated specimen and 26.5 vol% for the annealed specimen. This is considered to result from the molecular orientation formed in the surface layer of

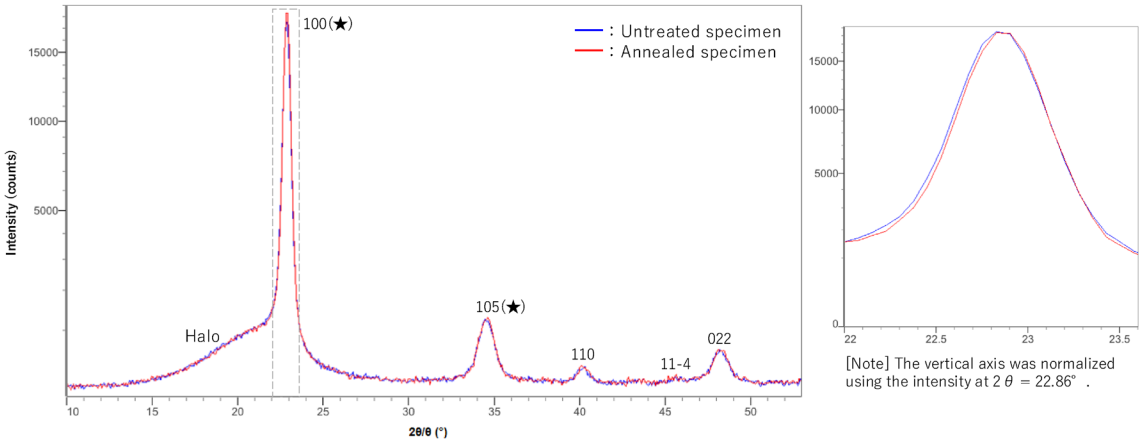

Fig. 4. Wide-angle X-ray diffraction patterns of the untreated and annealed specimens, and an enlarged view of the area between 2θ=22.0−23.6°, as indicated by the dashed line.

Table 3. $\theta/2\theta$ scan parameters.

Counting mode	2θ range	2θ step	Counting time
Fixed Time	10–53°	0.075°	8 sec/step

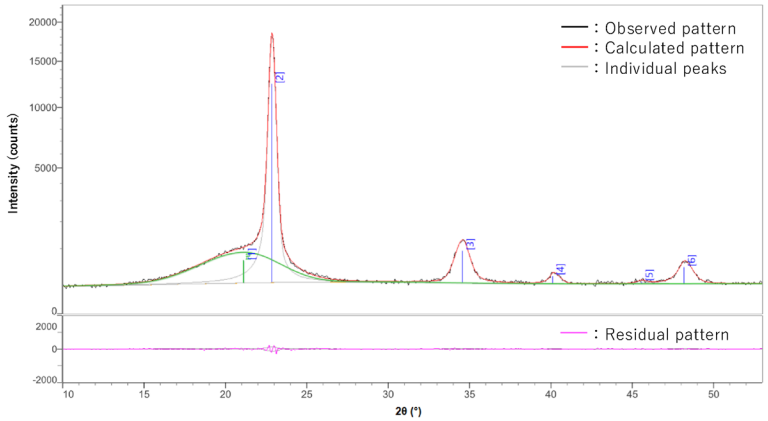

Fig. 5. Result of peak separation for the annealed specimen using the WPPF method.

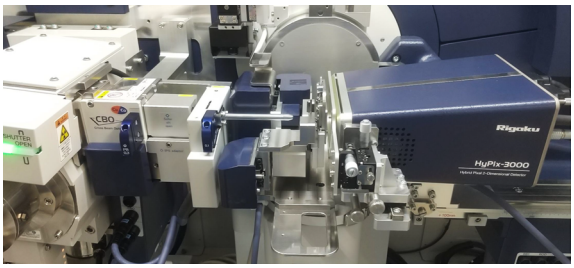

Fig. 6. Measurement optical system for the 2D-WAXS method using SmartLab.

the specimen, which is in contact with the mold during injection molding.

It should be noted that tensile stress measurements were conducted on the diffraction peaks of the (100) plane (2θ: 22.87°) and the (105) plane (2θ: 34.53°), as indicated by the star markers in Fig. 4. The results of the stress measurement are discussed in Section 4.2.2.

4.1.2. Transmission 2D Wide-Angle Scattering Measurement

The transmission two-dimensional wide-angle X-ray scattering method (WAXS) is highly effective for evaluating the degree of crystallinity and orientation in polymer materials. In two-dimensional measurements, diffracted X-rays can be observed as Debye rings, allowing for visual assessment of orientation states and the size of crystallites. Figure 6 shows the measurement optical system for the 2D-WAXS method using SmartLab. By positioning the two-dimensional detector close to the sample and performing transmission measurements, the full Debye rings over a certain 2θ range can be observed. The distance from the sample to the detector (camera length) is adjustable. In this study, the camera length was set to approximately 27 mm. Under these conditions, the measurable range was roughly 2θ: 7–36°. A micro-focused beam was formed using a ϕ0.3 mm pinhole and a ϕ0.1 mm collimator for the incident X-rays. The direct beam transmitted through the sample was blocked by a beam stopper positioned immediately before the detector.

Figure 7 shows the two-dimensional X-ray diffraction images measured by the 2D-WAXS method for the untreated and annealed polyacetal specimens. The X-ray exposure time for each 2D image was set to 5 minutes. The specimens were positioned so that the surface was perpendicular to the incident X-rays and the longitudinal direction of the specimen was aligned parallel to the normal direction of the sample stage. Figure 8 shows the one-dimensional patterns obtained by β-intensity conversion from the 2D images of the untreated and annealed specimens. The horizontal axis represents the β angle along the circumference of the Debye ring, and the vertical axis represents the diffraction intensity; data conversion was performed under the conditions listed in Table 4. The conversion range is indicated by a red frame in Fig. 7.

Table 4. Data processing parameters for β-intensity conversion from the 2D images.

hkl	2θ range	β range	β step
100	20.2–25.6°	0–360°	2°/step

Figure 7 shows continuous Debye rings in both the untreated and annealed specimens, indicating the formation of fine crystallites. In Figure 8, when the 6 o'clock position on the Debye ring is set as β=0° (with the counterclockwise direction as positive), both specimens show broad peaks at β=90° and β=270°. However, since the diffraction intensity is distributed over β=0–360°, this indicates that the molecular chains (the c-axis direction of the hexagonal lattice) are preferentially aligned along the MD direction, while the (100) plane exhibits weak orientation in the transverse direction of the specimen.

4.2. X-ray Stress Measurement

4.2.1. Tensile Testing Machine

The tensile-test attachment compatible with SmartLab, as shown in Fig. 9, was used for the tensile testing machine. The tensile-load range is 10–1000 N, which is sufficient to fracture polymer specimens. The tensile load is measured using a built-in load cell. The specimen is clamped at both ends, and the specimen is manually pulled in the longitudinal direction of the device using the supplied torque wrench. The attachment is compatible with scaled specimens A13 and A23 specified in JIS K7139, as well as Type V specimens specified in ASTM D638.

4.2.2. Tensile Stress Measurement (0D)

Tensile stress measurements were performed for the (100) and (105) diffraction peaks (2θ: 22.87° and 34.53°) of polyacetal. The measurement conditions for the side-inclination method are summarized in Table 5. Considering the viscoelastic behavior of polymers[4], the maximum applied stress was set to 20 MPa, and the stress was reduced in 4 MPa increments.

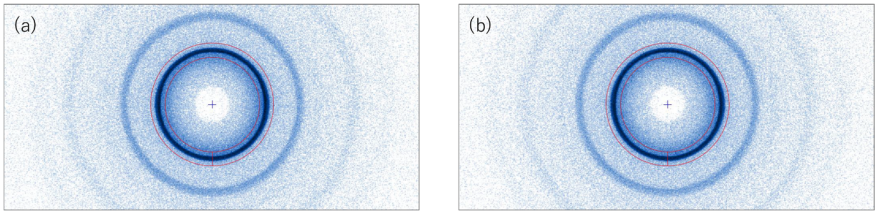

Fig. 7. Two-dimensional X-ray diffraction images measured by the 2D-WAXS method for the untreated (a) and annealed (b) specimens.

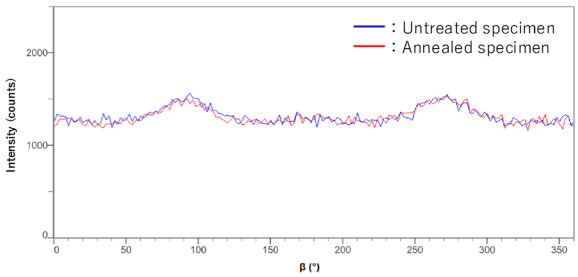

Fig. 8. One-dimensional X-ray diffraction patterns obtained by β-intensity conversion from the 2D images of untreated and annealed specimens.

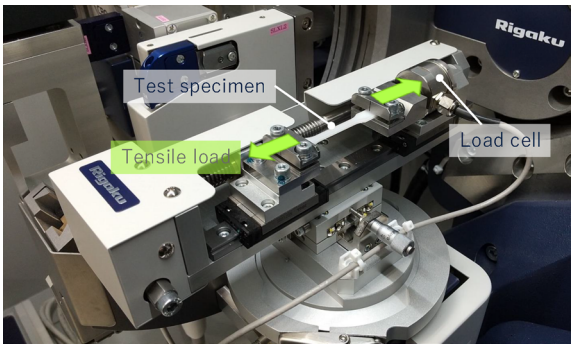

Fig. 9. Tensile-test attachment compatible with SmartLab.

Table 5. Stress measurement parameters by the side-inclination method.

(*hkl*)	2θ	2θ range	ψ range
(100)	22.87°	15–28°	0–45°, Div.6
(105)	34.53°	32–37°	0–45°, Div.6

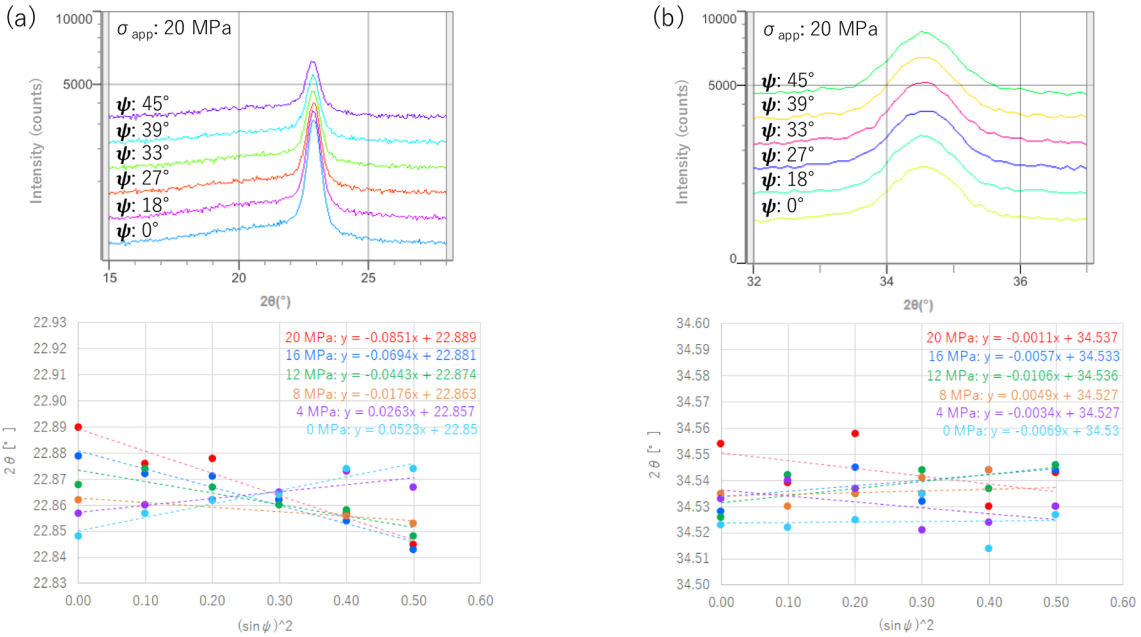

Fig. 10. Results of tensile stress measurements for the untreated polyacetal specimen.
Peak shift observed at 20 MPa and the 2θ–sin$^2\psi$ diagrams for the (100) plane (a) and (105) plane (b).

X-ray stress measurements were conducted at each load level during unloading. The maximum applied stress corresponds to approximately 30% of the tensile strength, to ensure that the measurements were within the elastic region. In addition, a strain gauge suitable for polymers was attached to the back surface of the specimen to simultaneously measure the strain induced by tensile loading. For these measurements, a uniaxial strain gauge (model KFP-2-120-C1-65 L1M2R), a strain measurement device (model EDX-10B/11A), and a bridge box (model DB-120C-2), all manufactured by KYOWA, were used.

First, Fig. 10 shows the results of tensile stress measurements for the untreated polyacetal specimen. Figure 10(a) shows the results for the (100) plane, and Figure 10(b) for the (105) plane, including the peak shift at the maximum applied stress (20 MPa) and the 2θ–sin$^2\psi$ diagrams for six stress levels. As shown in the lower panel of Fig. 10(a), the slope of the 2θ–sin$^2\psi$ diagram for the (100) plane changed in response to applied stress. Over the entire unloading process from the maximum applied stress, the vertical intercept (2θ) shifted by approximately 0.04°, indicating that even such a small peak shift could be detected. However, some scatter was observed in the linearity and intersection points of the regression lines in the 2θ–sin$^2\psi$ diagrams. In contrast, as shown in the lower panel of Fig. 10(b), the slope of the 2θ–sin$^2\psi$ diagram

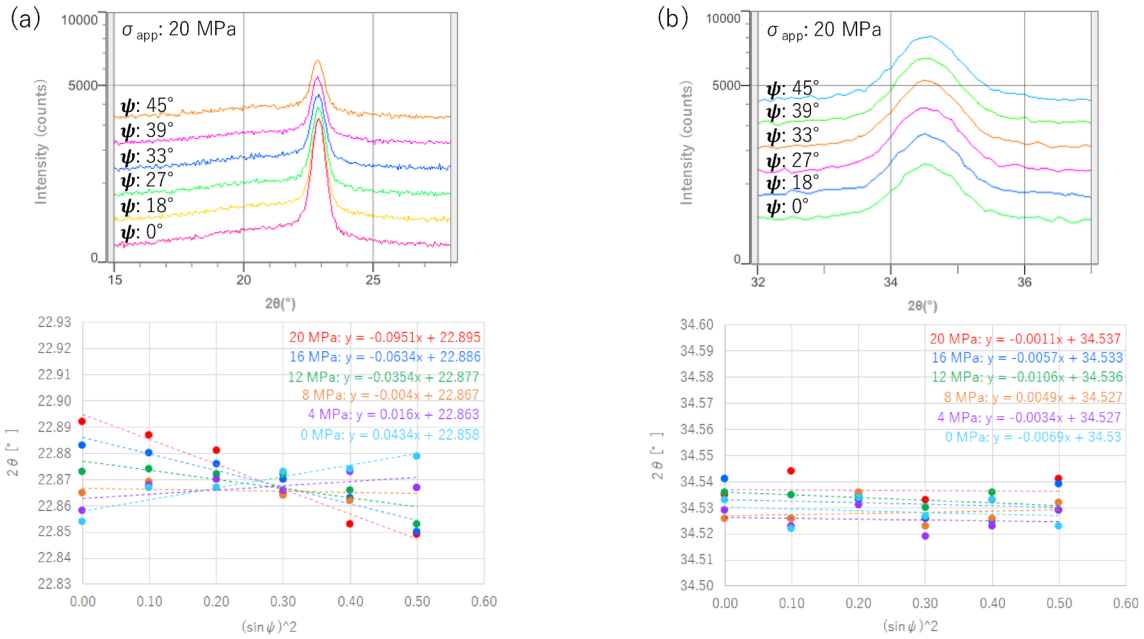

Fig. 11. Results of tensile stress measurements for the annealed polyacetal specimen.
Peak shift observed at 20 MPa and the 2θ–$\sin^2\psi$ diagrams for the (100) plane (a) and (105) plane (b).

corresponding to applied stress for the (105) plane remained unchanged.

Next, Fig. 11 shows the results of tensile stress measurements for the annealed polyacetal specimen. Similarly, the peak shift at the maximum applied stress of 20 MPa and the 2θ–$\sin^2\psi$ diagrams for six levels of applied stress are shown for both the (100) and (105) planes. As shown in the lower panel of Fig. 11(a), the 2θ–$\sin^2\psi$ diagrams for the (100) plane showed high linearity at each tensile load. Furthermore, the slope of the 2θ–$\sin^2\psi$ diagrams changed sequentially with increasing applied stress, and the regression lines generally intersected at a single point. Over the entire unloading process from the maximum applied stress, the vertical intercept (2θ) shifted by approximately 0.04°, and this shift was observed with higher precision compared to the untreated specimen. The intersection point of the regression lines represents the strain-free state, and its vertical axis corresponds to the $2\theta_0$ value. In contrast, as shown in the lower panel of Fig. 11(b), the slope of the 2θ–$\sin^2\psi$ diagram corresponding to applied stress for the (105) plane remained unchanged.

Here, we discuss the measurement results for the untreated and annealed specimens. Comparing the results for the (100) plane shown in Figures 10(a) and 11(a), it is evident that the scatter in the 2θ–$\sin^2\psi$ diagrams is reduced in the annealed specimen compared to the untreated specimen. This is attributed to the decrease in the full width at half maximum of the (100) diffraction peak in the annealed specimen, as shown in Fig. 4, resulting in improved precision in determining the peak position. On the other hand, as shown in Figs. 10(b) and 11(b), the slope of the 2θ–$\sin^2\psi$ diagram corresponding to applied stress for the (105) plane remained unchanged, irrespective of annealing treatment. This is considered to be due to differences in the crystal structure between the (100) and (105) planes. Further discussion on this point is provided in Section 4.3.

4.2.3. Determination of X-ray Elastic Constants

Using the results obtained from the tensile stress measurements, the X-ray elastic constant of polyacetal was determined[9]. Based on the fundamental equation of the $\sin^2\psi$ method shown in Eq. (2), a plot (M–σ_{app} diagram) was constructed, with the applied stress σ_{app} (calculated from the measured tensile load and specimen cross-sectional area) on the horizontal axis and the slope M of the 2θ–$\sin^2\psi$ diagram on the vertical axis. As shown in Eq. (5), the stress constant K can be obtained as the reciprocal of the slope M' of the regression line.

$$M = -\frac{2(1+\nu)}{E}\cdot\tan\theta_0\cdot\frac{180}{\pi}\cdot\sigma_{app}$$
$$M = M'\cdot\sigma_{app} = \frac{1}{K}\cdot\sigma_{app} \quad (5)$$

Figure 12 shows the M–σ_{app} diagrams for the (100) plane of the untreated and annealed polyacetal specimens. As seen in Fig. 12, both the untreated and annealed specimens show a linear relationship in the M–σ_{app} diagrams. In addition, consistent with the results described in Section 4.2.2, the scatter of the plots in the M–σ_{app} diagram is reduced for the annealed specimen compared to the untreated specimen. Comparing the coefficients of determination (R^2) for each linear regression analysis, the untreated specimen has a value of 0.9578, while the annealed specimen has 0.9977, indicating improved linearity due to annealing.

From Eq. (5), the stress constant K was calculated for both the untreated and annealed specimens, yielding −146.94 MPa/° for the untreated specimen

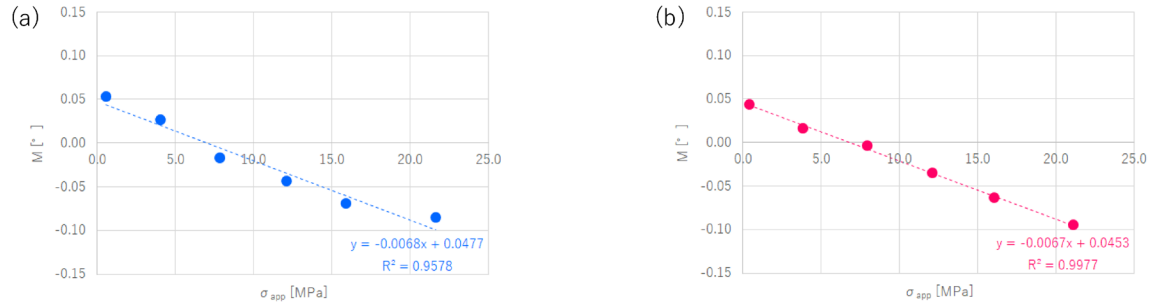

Fig. 12. M–σ_{app} diagrams for the (100) plane of the untreated (a) and annealed (b) specimens.

and −149.87 MPa/° for the annealed specimen. The annealed specimen exhibited a slightly higher degree of crystallinity than the untreated specimen, and the larger stress constant for the annealed specimen is consistent with this result. However, each plot shown in Fig. 12 represents a single measurement (N = 1), and error bars are not included. This is a subject for future work, and it will be necessary to increase the number of measurements to improve statistical accuracy.

4.3. Summary and Discussion of Analytical Results

As shown in Fig. 12, both the untreated and annealed specimens showed high linearity in the M–σ_{app} diagrams for the (100) plane. This result suggests that X-ray stress measurement of polyacetal can be performed with high accuracy for the (100) plane. In addition, the slope of the linear regression line in the M–σ_{app} diagram enabled experimental determination of the stress constant necessary for accurate stress quantification.

Here, we discuss the reason for the difference in the slope response to applied stress in the 2θ–$\sin^2\psi$ diagrams between the (100) and (105) planes[10]–[17]. As shown in Fig. 13, polyacetal has a hexagonal crystal structure in which molecular chains composed of [–CH_2O–] units are aligned along the c-axis. The (100) plane is a lattice plane along the a-axis, where the molecular chains are folded and aligned. Since this direction is governed by weak intermolecular forces, it is more susceptible to strain and thus exhibits greater response to applied stress. In contrast, the (105) plane is a lattice plane along the c-axis, where the molecular chains are aligned. This direction is dominated by strong covalent bonds, making it less susceptible to strain and resulting in minimal response to applied stress.

It has been reported that, in some polymers, the crystal elastic modulus differs by factors of several to several tens between the intermolecular (between-chain) direction and the covalent (along-chain) direction.[12], [16] Therefore, in X-ray stress measurement of crystalline polymers, it is important to appropriately select the diffraction peaks used for stress measurement, taking into account not only the strain sensitivity conditions dependent on the 2θ angle, but also the crystal structure of the polymer, since some peaks are suitable for stress measurement while others are not.

Furthermore, as described in Section 3.4, to achieve

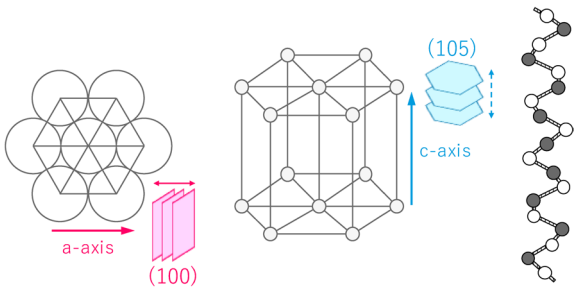

Fig. 13. (100) and (105) planes in the hexagonal crystal structure.

high-precision X-ray stress measurement of polymer materials, it is essential to use an X-ray diffractometer equipped with (1) highly parallel incident X-rays, (2) a measurement optical system with high angular resolution, and (3) a high-precision goniometer with a side-inclination axis. It is also important to check the optical axis alignment of the measurement system in advance by performing stress measurements under the same conditions as the test specimen using a stress-free sample such as LaB_6 powder. In practice, since the degree of crystallinity and orientation state of polymer materials are expected to vary depending on molding conditions, it is desirable, as described in this study, to first perform tensile stress measurements using test specimens made from the same material as the actual product, evaluate the feasibility and accuracy of X-ray stress measurement, and experimentally determine the X-ray elastic constants prior to evaluating the residual stress in actual products.

5. Conclusion

Polymer materials are expected to serve as lightweight and high-strength structural components. In this context, it is extremely important to evaluate material strength by multifaceted analyses of residual stress, crystallinity, and molecular orientation in polymers. The SmartLab X-ray diffractometer utilized in this paper enables a variety of analyses to be performed with a single instrument by easily switching to optimal measurement optics.

As for future prospects and challenges, it will be necessary to advance the evaluation of filler-reinforced materials, as well as other major engineering plastics in addition to polyacetal. Examples include crystalline polymers such as PA (polyamide), which is classified

as a general-purpose engineering plastic, and PEEK and PPS, which are classified as super engineering plastics. Furthermore, there is a significant need for the evaluation of amorphous polymers such as PC (polycarbonate) in future studies. However, the evaluation of residual stress in polymer materials still remains a subject of ongoing research. Further research is required to accumulate fundamental data and to deepen the understanding of residual stress evaluation in polymer materials.

Acknowledgments

The authors would like to express sincere gratitude to Professor Yoshiaki Akiniwa of Yokohama National University for his valuable advice and insightful comments on the measurements, data analysis, and interpretation of the results.

References

(1) W. Mizuno, Y. Hosono, Y. Maekawa, Y. Hamada, A. Yokoyama, and K. Tomari: *Kobunshi Ronbunshu*, **49** (1992), No.2, 125–132. [in Japanese]
(2) K. Takasa, N. Miyashita, S. Tachibana, and K. Takeda: *Zairyo (Journal of the Society of Materials Science, Japan)*, **54** (2005), No.1, 51–55. [in Japanese]
(3) K. Kawaguchi and Y. Tajima: *Kobunshi Ronbunshu*, **62** (2005), No.3, 124–130. [in Japanese]
(4) J. Watanabe [ed.]: Kobunshi, Maruzen, (2009), 31–40, 67–86, 137–168. [in Japanese]
(5) A. Okawa: *Kobunshi*, **9** (1960), No.7, 458–461. [in Japanese]
(6) T. Nishino: *Journal of the Adhesion Society of Japan*, **39** (2003), No.1, 24–29. [in Japanese]
(7) M. Kakuto: *Kobunshi*, **12** (1963), No.140, 814–819. [in Japanese]
(8) M. Takayanagi: *Kobunshi*, **20** (1971), No.230, 342–356. [in Japanese]
(9) K. Tanaka, S. Tokoro, Y. Koike, N. Egami, and Y. Akiniwa: *Zairyo (Journal of the Society of Materials Science, Japan)*, **63** (2014), No.7, 514–520. [in Japanese]
(10) A. Okawa: *Kobunshi*, **6** (1957), No.2, 86–89. [in Japanese]
(11) A. Okawa: *Kobunshi*, **6** (1957), No.3, 133–137. [in Japanese]
(12) T. Ito: *Kobunshi*, **13** (1964), No.142, 30–48. [in Japanese]
(13) T. Ito: *Kobunshi*, **34** (1985), No.11, 890–893. [in Japanese]
(14) S. Kogaya: *Sen'i to Kogyo (Journal of the Society of Fiber Science and Technology, Japan)*, **58** (2002), No.3, 68–73. [in Japanese]
(15) A. Toda: *Sen'i to Kogyo (Journal of the Society of Fiber Science and Technology, Japan)*, **63** (2007), No.12, 395–400. [in Japanese]
(16) H. Uehara: *Kobunshi Ronbunshu*, **64** (2007), No.8, 525–538. [in Japanese]
(17) D. Sawai: *Seikei Kako (Journal of the Japan Society of Polymer Processing)*, **19** (2007), No.10, 606–612. [in Japanese]
(18) https://www.polyplastics.com/Gidb/GradeListSelectGradeAction.do?id=1771